Theoretical Study of M^+-RG_2: (M^+= Ca, Sr, Ba and Ra; RG= He–Rn)

Anna Andrejeva[a], Adrian M. Gardner[a,b], Jack B. Graneek[a,c], W. H. Breckenridge[d]

and Timothy G. Wright[a]*

[a]School of Chemistry, University of Nottingham, University Park, Nottingham, NG7 2RD, U.K.

[b]Present address: Chemistry building, Department of Chemistry, Emory University, Atlanta, GA 30322, U.S.A

[c]Present address: Max-Planck Research Group "Structure and Dynamics of Cold and Controlled Molecules", Centre for Free Electron Laser Science, Building 99, Notkestrasse 85 D-22607 Hamburg Germany

[d]Department of Chemistry, University of Utah, Salt Lake City, Utah, 84112, USA

*To whom correspondence should be addressed. Email: Tim.Wright@nottingham.ac.uk

Abstract

Ab initio calculations were employed to investigate M^+-RG_2 species, where M^+ = Ca, Sr, Ba and Ra and RG= He–Rn. Geometries have been optimized, and cuts through the potential energy surfaces containing each global minimum have been calculated at the MP2 level of theory, employing triple-ζ quality basis sets. The interaction energies for these complexes were calculated employing the RCCSD(T) level of theory with quadruple-ζ quality basis sets. Trends in binding energies, D_e, equilibrium bond lengths, R_e, and bond angles are discussed and rationalized by analyzing the electronic density. Mulliken, natural population, and atoms-in-molecules (AIM) population analyses are presented. It is found that some of these complexes involving the heavier Group 2 metals are bent whereas others are linear, deviating from observations for the corresponding Be and Mg metal-containing complexes, which have all previously been found to be bent. The results are discussed in terms of orbital hybridization and the different types of interaction present in these species.

1. Introduction

Weak electrostatic interactions have been studied abundantly in the past two decades, both experimentally and theoretically. M^+-RG species, where M^+ is a metal cation and RG is a rare gas atom, are prototypical systems for the study of solvation.[1] Previously, our group has studied extensively the whole series of M^+-RG complexes, where M = Group 1 metal,[2,3,4,5,6] Group 2 metal[7,8,9] and Group 13 metal.[10,11,12,13] It was shown that for the Group 1 complexes the interactions were almost entirely physical in nature, a fact reflected in their relatively low interaction energies. In contrast, for the M^+-RG complexes where M = Group 2 metal, much higher dissociation energies were observed. This has been attributed to hybridization between the outer s orbital on the metal cation and its lowest unoccupied p or d orbital.[7,8,9] This hybridization occurs as the RG atom approaches the metal centre and facilitates the movement of electron density away from the incoming RG, minimizing electron repulsion and, concomitantly, increasing attractive forces.

Bauschlicher et al.[14] reported one of the earliest studies on M^+-RG_2 systems. Their study focused on RG = Ar, and M = Li, Na, Mg, V, Ni and Cu. The study concluded that the Li^+-Ar_2 and Na^+-Ar_2 complexes were linear, while Mg^+-RG_2 complexes were bent – conclusions that we have corroborated and extended in our previous work.[15] In that work, we showed that the Li^+-RG_2 and Na^+-RG_2 complexes have very flat angular potentials, but the global minimum was the linear structure in each case; in contrast, the Group 2 M^+-RG_2 complexes for M = Be and Mg were found to be of C_{2v} symmetry. The explanation for the difference in the equilibrium geometry for the Group 2 containing species was the occurrence of sp hybridization of the

outermost occupied s orbital on the metal centre. Such hybridization makes it favourable for the second RG atom to approach the metal centre from the same side as the first, owing to the reduction in electron density and so, notwithstanding possible RG…RG repulsion, both atoms approach from the same side. In the present work we extend our previous study to the M^+-RG_2 complexes containing a heavier Group 2 metal cation (M = Ca–Ra), to examine if these bent geometries persist.

Very little work has been done experimentally or theoretically on these heavier metal M^+-RG_2 complexes.[16] In 2001, Duncan and co-workers recorded mass-selected, photodissociation spectra of the Ca^+-Ar_2 complex;[17] however, since their spectrum was not rotationally resolved, whether the geometry was linear or bent was not conclusively established. Quantum chemical calculations reported in the same work confirmed that a bent equilibrium structure was preferred at the MP2/aug-cc-pVQZ level of theory; however, because of basis set superposition error, and the very small energy differences, this was not considered a conclusive result by the authors. Quite recently, density functional theory (DFT) calculations on Ca^+-RG_n (n = 1–4, RG = He, Ne and Ar) have been reported by Jalbout and Solimannejad.[18] B3LYP/6-311+G(3df) geometry optimizations were performed, with all three Ca^+-RG_2 complexes being concluded to be bent, with bond angles of 58°, 67° and 76°, for RG = He, Ne and Ar, respectively. Additionally, binding energies and harmonic vibrational frequencies were reported for all species, which will be commented on below. We are aware of no other studies on Ca^+-RG_2 complexes.

Photofragmentation electronic spectra of Sr^+-Ar_n (n = 2–8) complexes, have been recorded by Fanourgakis et al., [19] with a more detailed study on Sr^+-Ar_2 published soon afterwards.[20] This group also undertook quantum chemistry calculations, RCCSD(T)/d-aug-cc-pVDZ level, obtaining a structure of C_{2v} symmetry with an equilibrium bond angle of 65.4° and R_e = 3.629 Å. No other studies on strontium-containing M^+-RG_2 complexes appear to be available.

There do not appear to be any published studies on the M^+-RG_2 complexes for M = Ba or Ra, and so the present results appear to be the first such reported.

2. Computational Details

All of the calculations were undertaken with the MOLPRO[21] suite of programs. Geometry optimizations of the titular species were performed at the MP2 level employing triple-ζ quality basis sets. Angular scans were undertaken, also employing triple-ζ quality basis sets, where at each fixed angle the internuclear distances were independently optimized to yield a minimum energy path along the angular coordinate. Single-point RCCSD(T) binding energy calculations were undertaken at the MP2-optimized geometry with quadruple-ζ basis sets. We did not correct these for basis set superposition error (BSSE), since for the corresponding M^+-RG complexes we have seen that for basis sets of quadruple-ζ or better, the RCCSD(T) dissociation energies are only slightly (< 5%) affected by BSSE.

For He and Ne, standard aug-cc-pVTZ basis sets were utilized, whereas for Ar we employed standard aug-cc-pCVTZ basis sets. For the heavier rare gases, Kr, Xe and Rn, the small-core relativistic effective core potentials (ECPs)[22] ECP10MDF, ECP28MDF and ECP60MDF respectively were used, along with the corresponding aug-cc-pwCVTZ-PP basis sets.[23] The electrons of He were correlated, as were all non-ECP electrons of the Ca, Sr, Ba and Ra cations; only the 1s orbital of Ne, and the 1s, 2s and 2p orbitals of Ar were frozen. For Kr, Xe and Rn, only the innermost s and p orbitals that were not included in the ECP, were frozen. For Ca, Sr, Ba and Ra atoms, aug-cc-pwCVTZ-PP[24] valence basis sets were employed with ECP10MDF, ECP28MDF, ECP46MDF and ECP78MDF effective core potentials,[25] respectively.

Three population analysis methods were also employed in this work. Mulliken population analysis was used as implemented in Gaussian 09 whereas the AIM analyses utilized the AIMAll software package using WFX files produced by Gaussian 09.[26] NPA analyses were performed using the NBO 6.0[27] software package.

3. Results and Discussion

A. Geometries

Table 1 shows the optimized geometric parameters for all of the titular complexes. Every one of the Ca^+-RG_2 complexes exhibit bent minimum geometries, similar to the Be^+-RG_2 and Mg^+-RG_2 species studied previously.[15] The M^+…RG internuclear distances in the triatomic complexes, R_{e2}, decrease at first from He to Ar and then increase for the heavier rare gases, with Ca^+-Ar_2 having the minimum bond length; this is represented in Figure 1. As may be seen, essentially the same trend is observed for the diatomic M^+-RG complexes. These unusual trends have been attributed[7] to a delicate balance between the increasing ion/induced-dipole attraction arising from an increase in the polarizability of RG atom with atomic number, and an associated increase in electron repulsion owing to the increasing number of electrons. It is notable that for the Ca^+-He_2 complex, the optimized bond lengths are not equal. Attempts were made to optimize the geometry with C_{2v} symmetry; however, this led to a higher energy structure (although by only +0.4 cm^{-1}) with R_{e2} = 4.352 Å; for all other complexes, a C_{2v} structure was obtained. For Ca^+-Ar_2, the R_{e2} value of 3.291Å is in fair agreement with the value from ref. 14 of 3.172Å obtained at the MP2/aug-cc-pVQZ level; our value for the optimized angle for the Ar–Ca^+–Ar complex is within 1° of that in ref. 14. In contrast, the DFT results of ref. 18 for the two lighter complexes, Ca^+-He_2 and Ca^+-Ne_2 are in somewhat poor agreement with the present results: although there is agreement that the equilibrium geometry is of C_{2v} symmetry, the bond angles are significantly larger than those here. There is, however, good agreement for the Ca^+-Ar_2 bond angle.

For the Sr^+-RG_2 species, only the lighter three complexes have bent equilibrium geometries, as shown in Table 1, with the three heavier rare gas complexes preferring a linear configuration. The bond length trend here (see Figure 1) is the same as for Ca^+-RG_2 (and Ca^+-RG) complexes with the initial decrease and then increase in the equilibrium internuclear separation with increasing atomic number of the rare gas; indeed, this trend is also seen for both of the other two M^+-RG_2 series of complexes. In ref. 20, the Sr^+-Ar_2 species was found to be of C_{2v} symmetry with an Ar–Sr^+–Ar equilibrium bond angle of 65.4° and R_e = 3.629 Å; these were calculated at the RCCSD(T)/d-aug-cc-pVDZ level of theory. Both of these values are in good agreement with our calculated MP2/aug-cc-pVTZ parameters despite the different levels of theory, with the angles being almost identical, but their bond length is 0.13 Å longer than ours.

In the Ba^+-RG_2 complexes, only the species with RG = He and Ne prefer a bent geometry, whereas geometries for Ra^+-RG_2 complexes break the trend again by having optimized linear geometries for Rn only as shown (see Table 1).

We shall discuss the trends in geometry in the below in terms of electrostatic attraction and repulsion terms, as well as hybridization. For the latter, if sp hybridization occurs, then this favours a bent geometry, while sd hybridization favours a linear geometry. In both cases, the cost of the hybridization process must be offset by other terms, such as an increase in electrostatic attraction and a decrease in electron repulsion terms, and such effects will be discussed in more detail below for the different species.

B. Angular Cuts Through the Potential Energy Surfaces

While comparing the geometry trends previously for Group 1 (M = Li and Na) and Group 2 (M = Be and Mg) complexes[15] it was ascertained that the lightest Group 1 M^+-RG_2 complexes were linear while the lightest Group 2 M^+-RG_2 complexes were bent at the global minima for all RG. Cuts through the potential energy surface (see Figs 5 and 6 of ref. 15) showed that the potentials of the Group 1 complexes were very flat along the angular coordinate (where the bond lengths had been optimized at each point), with the M = Na complexes exhibiting a shallow bent local minimum, but with the global minimum still being linear (for M = Li^+, no such bent local minimum was evident). In contrast, for the Group 2 complexes, M = Be and Mg, there was a significant bent global minimum, with a saddle point at the linear geometry.

In the present work, Figure 2 shows angular cuts through the M^+-RG_2 potential energy surfaces for M = Ca–Ra and RG = He, Ar and Xe. Potential energy surface cuts are shown for angles from 35° to 325° with the internuclear distances being independently optimized. (The zero on the interaction energy axis is for the M^+-RG + RG asymptote.) Figure 2a shows M^+-He_2 angular plots where a bent global minimum dominates, but with a shallow linear local minimum being evident in all cases. In the case of the RG = Ar complexes (see Figure 2b), there are also both bent and linear minima, with the bent geometry being the global minimum for all M^+-Ar_2 complexes, except for M = Ba, which is linear. For RG = Xe (Figure 2c) there is again a linear global minimum for the M = Ba complex, but also for M = Sr; again, Ca^+-Xe_2 and Ra^+-Xe_2 each have bent global minima.

Energy differences between the linear and bent structures were calculated, and these are shown in Table 2. For the lightest two metals, Be^+ and Mg^+, all of the M^+-RG_2 species have a bent global minimum and so all values are negative. In both cases, however, there is a clear general trend of increasing negative values for RG = He–Rn, making the bent structure more and more favoured as the atomic number of the RG atom increases. If we now look at the Ca^+-RG_2 – Ra^+-RG_2 species, we can see that linear–bent energy differences are all negative for RG = He and Ne, but then differences arise between the species. For M = Sr and Ba with the heavier RG atoms, linear global minima result, but for M = Ra, only Ra^+-Rn_2 is linear. There is, however, no monotonic trend in the linear-bent energy differences, with oscillations in the calculated values. For the Ca^+-RG_2 species, all structures remain bent, although the barrier for Ca^+-Rn_2 is less than that for Ca^+-Xe_2. It is clear that there are some subtle issues here, and we shall discuss these below in terms of a balance between hybridization, ion-dipole and higher-order electrostatic interactions, and repulsion terms.

Harmonic vibrational frequencies were also calculated and are presented in Table 3. For the linear structures, four real frequencies (with two being degenerate) were obtained, whereas bent structures resulted in three real frequencies. The values may all be seen to be of the order of tens of cm^{-1} and so these harmonic frequencies can only be taken as indicative. The flatness of the potential energy curves (PECs) was also evident in that tight convergence criteria were needed during the optimization procedures in order to obtain all real vibrational frequencies.

C. Dissociation Energies

The energy for the removal of a single RG atom from M^+-RG_2, D_{e2}, was calculated for all complexes studied and was compared to the dissociation energy of the M^+-RG complexes, D_{e1}. The results are presented in Table 1, along with D_{e2}/D_{e1} ratios. As well as reporting the MP2/aug-cc-pVTZ dissociation energies, we also calculated D_e values using single-point RCCSD(T)/aug-cc-pVQZ calculations at the respective MP2-optimized geometries. Relatively good agreement for D_{e1} and D_{e2} was obtained between the two methods, with energies for most complexes being within 10%, with the RCCSD(T) values being the greater. It was shown in ref. 12 that both a higher level of theory and larger basis sets are needed to describe both attractive

and repulsive interactions accurately for these kind of systems; additionally, it was shown by the Duncan group that using MP2 theory and including both valence and core electron correlation, with large basis sets, can reproduce experimental results for dissociation energies.[17,28]

There is a monotonically increasing trend in D_{e2} for all of the M^+-RG_2 complexes with increasing atomic number of RG – see Figure 3. This is both the same as the pattern previously observed for the Be^+-RG_2 and Mg^+-RG_2 series,[15] as well as for the D_{e1} variations in the M^+-RG complexes.[7,8,9] An increase in binding energy indicates that the increasing trend in the attractive forces is dominating over the repulsive ones, and occurs here regardless of whether the global minimum geometry is bent or linear.

It is interesting to note that the D_{e2}/D_{e1} ratios are significantly different here for the heavier M^+-RG_2 complexes compared to those with M = Be and Mg.[15] In ref. 15 it was seen for the Be^+–RG_2 complexes that D_{e2}/D_{e1} was very close to 1.0 for RG = He and Ne, while for RG = Ar–Rn, values close to 0.5 were observed. This was explained in terms of the small size of beryllium cations, noting that the hybridization and shift in electron density away from the incoming RG atoms is allowing an effective charge significantly higher than $+e$ to be experienced. As a consequence, the heavier RG atoms are being pulled significantly closer to the metal centre than would otherwise be the case, and this leads to significant repulsion from the RG atoms, which are being forced together. As such, the binding energy of the second RG atom is significantly reduced compared to that in Be^+-RG. (This also indicates that there is close-to-maximal hybridization on the metal centre already in Be^+-RG, so that the second RG atoms does not exacerbate this effect.) In the Mg^+-RG_2 complexes a similar effect is seen, but the D_{e2}/D_{e1} ratios are slightly larger than 1.0 for RG = He and Ne, and values decrease from 0.9 in Mg^+-Ar_2 to 0.75 in Mg^+-Rn_2. These values seem to suggest a slightly enhanced hybridization for RG = He and Ne as a result of the presence of the second RG atom, but for the heaver RG complexes, this is outweighed by the increasing repulsion. This repulsion is smaller than that in the case of the Be^+-RG_2 complexes owing to the larger size of the magnesium cations.

For the complexes in the present work we see markedly different D_{e2}/D_{e1} values. Again, we see values > 1.0 for the M^+-RG_2 complexes with the lightest RG atoms, and for M = Ca and Sr, we again see D_{e2}/D_{e1} values fall below 1.0 and slowly decrease, with final values of 0.85 and 0.89 for M = Ca and Sr, respectively, compared to the values of 0.50 and 0.75 for M = Be and Mg, respectively. The explanation for these values is the same as just outlined, with the larger asymptotic values for M = Ca and Sr coming from the larger size of these metal cations. Finally, we note that all of the D_{e2}/D_{e1} ratios for the two heaviest M^+-RG_2 series, Ba^+-RG_2 and Ra^+-RG_2 are ≥ 1.0, possibly due to an enhanced effect from the hybridization produced by the presence of the second RG atom in M^+-RG_2 compared to M^+-RG. We suggest that this occurs because of the larger, more polarizable nature of these two metal cations. We note that the D_{e2}/D_{e1} values for Ra^+-RG_2 are lower than those of the corresponding Ba^+-RG_2 complexes, which can be attributed to the lanthanide contraction, and relativistic effects, leading to a lower polarizability of radium cations compared to barium cations – see Table 4.

D. Atomic Charges

In Table 5 we present the results of three population analyses: Mulliken,[29] natural population analysis (NPA)[30] and atoms-in-molecules (AIM),[31] for each of the titular species; additionally, we perform the same analyses using the same basis sets for the M^+-RG dimers for comparison. [Only the charges on the metal centre, q_M, are shown, with the charge on the RG atom being $(1\text{-}q_M)/2$.] The values were obtained using the MP2 method with triple-ζ basis sets at the optimized geometries given in Table 1. From Table 5, it is clear that there is little charge transfer in the M^+-RG_2 complexes involving the lighter rare gas atoms, and this is a consistent picture from all three methods. However, for the M^+-RG_2 complexes involving the heavier rare

gas species, both NPA and Mulliken analyses predict some charge transfer, particularly for Sr^+-RG_2 and Ba^+-RG_2 complexes and the corresponding M^+-RG dimers. In contrast, the AIM values, in bold in Table 5, suggest minimal charge transfer. Comparison with the values for the M^+-RG complexes shows that there is very little difference between the two types of species, with just an enhancement seen in the corresponding triatomic complexes of the minor charge transfer. In our previous paper,[15] we concluded that the AIM charges were likely the more reliable; in any case, overall the suggestion is that the interactions in the present species are mostly physical (i.e. the interactions can be described by electrostatic, multipole models)[1] and can be viewed as non-covalent — more discussion of these points will follow.

E. Molecular Orbital Contours, Population Analysis and Geometry Rationalization

In this subsection we shall address the trends in geometry observed and attempt to rationalize them. We have already given the observed global geometries in Table 1, shown the trends in the energy difference between bent and linear structures in Table 2, and indicated that the final observed global structure depends on a number of energy terms: the cost of hybridization and whether this can be offset by increases in electrostatic interaction terms and/or a decrease in repulsion terms between the metal cation and the rare gas atoms; and additionally, the effect of the interaction between the RG atoms. We explore these ideas further, initially concentrating on information obtained from molecular contour plots and population analyses.

In Figure 4 we present contour plots of the HOMO obtained from the Hartree-Fock (HF) wavefunction, calculated at the two minimum energy positions: linear and bent for RG = He, Ar and Xe. We have found that the HF contours are extremely similar to contour plots of natural orbital density at the correlated level, as long as the geometry used is that optimized using a correlated method. To indicate which contours correspond to the global minimum, we have identified these by underlining the chemical formula. Looking first at the contours of the bent structures on the left-hand side of the figure, we can see that there is essentially no contribution from He for the M^+-RG_2 complexes, and the HOMO is just the outermost *n*s orbital of the M^+; there is a very similar picture for the M^+-Ne_2 complexes (not shown). It is noteworthy that the complexes with RG = He or Ne are all bent, and all have very little hybridization, with the HOMO being made up almost exclusively from the outermost occupied *n*s orbital on the metal centre. We also note that the optimized RG…RG distance in the complex is very similar to that in the isolated RG_2 diatomic. Hence, we conclude that here the M^+-He_2 and M^+-Ne_2 complexes are best described as an RG_2 unit interacting with the metal cation.

For the heavier Ca^+-RG_2 and Sr^+-RG_2 complexes a picture reminiscent of that of the Be^+-RG_2 and Mg^+-RG_2 complexes is seen, with electron density located on the side of the metal cation opposite to the approaching RG atoms. For the corresponding Ba^+-RG_2 and Ra^+-RG_2 complexes, the contour plots are similar, but there is evidence for electron density building up at the sides of the metal. At this stage it will be useful to look at the natural bond order (NBO) populations.

Table 6 summarizes the output of NBO analyses undertaken with the NBO 6.0 software[27] for all of the M^+-RG_2 (M = Ca–Ra) complexes at both bent and linear geometries, and for M = Be, Mg at the bent minima reported in our previous paper.[15] It may be seen that for the Be^+-RG_2, Mg^+-RG_2 complexes, hybridization occurs between outer s and p orbitals, but with 92–100% of the orbital character coming from the s orbital. As may be seen, for M = Ca, Sr, there is very little contribution from the higher angular momentum orbitals; however, there are minor contributions, and they may be discerned in the contour plots. These comprise both p and d orbital contributions, with the p contributions giving rise to distortion away from the incoming RG atoms, and the d orbitals moving a small amount of the electron density to the sides. For Ba^+-RG_2, the

amount of d orbital involvement is now sizeable and leads to significant sideways movement of electron density. Interestingly, although the amount of d orbital involvement for Ra^+-RG_2 is now much reduced (and apparently not much more than for the M = Ca and Sr cases), the diagrams also exhibit clear movement of electron density off-axis.

We now move to the linear geometry contour plots on the right-hand side of Figure 4. Again, for RG = He, there is nothing very exceptional to note, with the HOMOs looking very much like the outermost *n*s orbitals on the metal centre; there is perhaps just an inkling of a slight flattening of the contour by the approaching He atoms for M = Ba and Ra. Much more noteworthy are the plots for RG = Ar and Xe. Here, we see distinct "off-axis" electron density forming, in an analogous manner to that seen in the corresponding diatomic M^+-RG complexes;[7] this arises from sd hybridization. Looking again at Table 6, we can see that the NBO analysis is showing that there are considerably more d orbital contributions in these linear orientations than there were for the bent ones; we note that this d character comes from the d_{z^2} orbital.

To discuss the interactions, it is useful to consider the polarizabilities of the RG atoms and the metal cations, and also the excitation energies to the lowest doublet states of the metals, for sd hybridization purposes. For the RG polarizabilities, some values are cited in ref. 1, and others are taken from ref. 32; for the metal cations, again some values are taken from ref. 1, with others from ref. 33. For the atomic excitation energies, values from the NIST online data resource are employed.[34]

We can partially rationalize the d orbital involvement in the heavier species from the atomic excitation energies (see Table 4), where the lowest energy orbitals are the *n*d ones, with the d orbitals of Ba^+ being particularly low. Thus, a key parameter in determining whether the lowest-energy structure is linear or bent is the ease of hybridization, which depends on the energy required to mix in d character. Clearly, however, this is not the whole story as Ba^+-He_2 and Ba^+-Ne_2 are bent. Another part of the rationale is that the cost of hybridization needs to be paid back, and for the smaller RG atoms their very low polarizability means that the resultant charge/induced-dipole interaction is not high enough to offset this. Once we get to the more polarizable Ar, then it becomes energetically favourable for sd hybridization to occur in Ba^+-Ar_2 and so we obtain a linear global minimum, and similarly for RG = Kr–Rn; for Sr^+, where the d orbitals are higher in energy (Table 4), the higher polarizability of RG = Kr–Rn are required to obtain linear global minima. Still, however, this does not explain the whole trend, and so we look at the hybridization in more detail.

As noted, the linear geometries can be explained by the sd_{z^2} hybridization, where destructive interference occurs between the s orbital and the lobes of the d_{z^2} orbitals along the *z* internuclear axis; this reduces the electron density making it favourable for two RG atoms to come in at a linear geometry in order to get closer to the cationic core and feel more strongly the ion/induced-dipole interaction. Concurrently, constructive interference between the "doughnut" of the d_{z^2} orbital and the s orbital takes place, allowing electron density to build up off-axis, resulting in the two "lobes" seen in the planar cut in Figure 4. Interestingly, there can be seen to be d orbital involvement in the bent structures as well, suggesting that the picture is not as straightforward. We know that the M^+-RG complexes exhibit sd hybridization, moving electron density off-axis. Here there is a balance between the cost of sd hybridization and the "payback" of the RG atom being able to get closer to the metal cation, and the exposure of more of the doubly-charged, M^{2+}, core. Thus, with the lower d orbitals, we see more sd hybridization for Ba^+-RG species than for the others.[7,9] Once a second RG atom approaches, the situation is less clear, as both RG atoms cannot favourably approach from the same side in a linear orientation. Hence, if they do approach from the same side, then the best approach is each along a nodal surface that forms by the cancellation of electron density when the amplitude of the s and d wavefunctions just match. There will be some compromise here, as the RG atoms also can exhibit steric repulsion. However, in all cases, a minimum energy does appear in this position and, further,

as evinced by the RG–RG distances in the complex, the final geometry essentially has the RG atoms at their equilibrium position in the isolated RG_2 system. To understand what happens next, we refer the reader to Figure 5: here we show the evolution of the HOMO as the RG atom moves from the bent orientation to the linear one for Ba^+-Xe_2. Here we can see that as we move away from the bent minimum, there is a barrier as the RG atom moves away from the nodal position, then a lowering of energy as the RG atom passes over into the collinear position to form the RG-M^+-RG geometry. At this point, both RG atoms can interact with the metal cation, and further electron density can be transferred from the internuclear regions through sd hybridization, into the off-axis position, essentially by adding in more d_{z^2} density, leading to further destructive interference from the lobes, and further constructive interference in the "doughnut" – this will occur as long as the sd hybridization costs can be repaid.

The above explains the form of the HOMOs seen, and the form of the angular plots, but it does not wholly explain the observed global minima. However, a large clue is seen from the HOMO plots in Figure 4, recalling that the underlining indicates the global minima. Looking at the plots for the linear structures, we see that for Ba^+-Ar_2 and Ba^+-Xe_2 there are no contours passing through the collinear region, in contrast to the corresponding M = Ca species, thus for the latter there is more electron repulsion along the collinear direction than there is in the former. For Sr^+-Ar_2 and Ra^+-Ar_2 we see such a contour, and the global minimum is bent. There is a little more subtlety for Sr^+-Xe_2 and Ra^+-Xe_2: for the former, the lack of a contour through the linear region is in line with the observed linear structure; however, for Ra^+-Xe_2 no contour exists, yet the global minimum is bent. First we note that the bent-linear energy difference for Ra^+-Xe_2 is very small at only 11 cm^{-1}, showing that this is a quasilinear molecule (this may also be seen from the angular plots in Figure 2c); secondly, we note that there is a bending of the contour towards the linear region, apparently just enough to destabilize the linear structure relative to the bent one. For Sr^+-Xe_2 the situation is essentially reversed in that it is still a quasilinear molecule as may be seen from the angular plots and small bent-linear energy difference, but also we can see that there is slightly less bending of the contour in Figure 4 towards the linear position, and so the linear geometry is just more stable than the bent.

Clearly, whether the destructive interference along the linear direction is sufficient to stabilize the linear structure or not depends on: the magnitude of the outermost *n*s wavefunction; the cost of "enough" sd hybridization to reduce this s electron density; and whether the cost of this hybridization can be paid back by the resulting reduction in electron repulsion and increase in the attraction of the RG atoms to the metal cation. Thus, for the Ca^+-RG complexes, the s-d energy gap is too high for sufficient hybridization to occur which could allow the linear electron density to fall sufficiently to favour the linear structure. For the Sr^+-RG_2 complexes, the s electron density is slightly more diffuse leading to greater ease of reducing the electron density by sd hybridization, but this also leads to a higher polarizability of Sr^+ (Table 4), which increases the dispersion interactions. Thus we find that for the two most polarizable RG atoms, Xe and Rn, the Sr^+-RG_2 complexes are linear, despite the slightly higher cost of sd hybridization owing to the more energetically distant 4d orbitals (see Table 4). For Ba^+-RG_2, similar considerations arise regarding the large size of the barium 6s orbital and increased polarizability, but now the cost of hybridization is much reduced owing to the energetically proximate 5d orbitals (Table 4) and so we see that for RG = Ar–Rn linear Ba^+-RG_2 structures result. Finally, we move onto M = Ra, where we note the effects of the lanthanide contraction and relativistic effects. These lead to the 7s orbital being more contracted than may be expected, and so Ra^+ has a lower polarizability than might be expected – Table 4, and so it is harder to cancel out electron density along the linear directions via sd hybridization. Thus, even though the cost of sd hybridization is expected to be less than that of the strontium complexes (Table 4), there is more sd hybridization required to counteract the higher 7s electron density. These are likely simplistic arguments, as

clearly a number of different factors are operating simultaneously, but these arguments seem to rationalize the observed trends.

As noted, in Table 2 we present the bent-linear energy differences. For the heavier species, there is no clear trend in the energy differences. The differences are somewhat small for M = Sr and Ra, in line with the very shallow curves seen in Figure 2 for these species; the barrier to linearity is also seen to be relatively small. This suggests a subtle balance between the energy cost of hybridization versus the energetic advantage of having done so (increased attraction/reduced repulsion), and whether the global minimum is linear or bent is hard to predict. For M = Ca, we see that there is a monotonic increase in the bent-linear energy difference from RG = He to Xe, but the changes are somewhat erratic. The suggestion is that the increasing polarizability of the RG atoms with atomic number is the key variable, but that this cannot outweigh the significant cost of providing enough sd hybridization to make the linear structure more energetically favourable.

The strongest-bound complexes are those involving barium, with the dissociation energies in Table 1 and the plots in Figure 3 showing that for the RG = Ar–Rn species these complexes are unusual compared to the other species. This undoubtedly rests with the very low-lying unoccupied 5d orbitals, meaning that the cost of hybridization is low and can be readily offset against the reduction in repulsion and increase in attraction that results. This gives the much higher degree of d involvement in the HOMO (Table 5, Figure 5), and so the much-increased stability of the linear structure (Figure 3, Table 2). It is interesting to note (Table 1, Figure 3) that the Ba^+-He_2 and Ba^+-Ne_2 complexes have the lowest binding energy, with the difference being very small compared to the M = Ra analogues, but more significant compared to M = Ca and Sr. The contour plots of the HOMOs in Figure 4 suggest that the electron density is higher further out for these two species, and so it seems the repulsion is higher, reducing the overall interaction energy.

4. Further Discussion and Conclusions

In the present work, it has been seen that the Group 2 complexes exhibit a mix of bent and linear equilibrium geometries, whereas extrapolation from our previous results[15] on Be^+-RG_2 and Mg^+-RG_2 would have led to the conclusion that a bent geometry would have occurred for all of the M = Group 2 metal species. For the M = Be and Mg complexes, the bent minimum geometry is attributed to sp hybridization on the metal centre, and there is some evidence of this also here at the bent geometries; in contrast, a linear geometry is attributed to sd hybridization between outer singly-occupied s orbital on the metal centre and the formally unoccupied d_{z^2} orbital. As we have shown, although there is a tendency for the complexes with both M and RG having a high atomic number to be linear, for the other species there is a subtle balance between the cost of sd hybridization, and whether this can be offset against the reduction in repulsion and increase in attraction. For many of the species the difference between the linear and bent structures is rather small, as are the barriers to linearity (see Figure 2); thus, a wide range of geometries are likely to be sampled, even at the zero-point vibrational level (see the representative, harmonic vibrational frequencies in Table 3). The HOMO contour plots of orbital wavefunctions, Figure 4, provide insight into the behaviour of these systems while NBO analysis supports the idea of sd hybridization being the crucial factor here.

AIM population analyses indicated that there was very little charge transfer from the metal cation onto the RG atom for any system; this is in line with the contour plots, which indicate only a hint of covalent character being present in these systems. Another test for covalency is the evaluation of the total local energy density parameter, $H(R)$, at a bond critical point; if this is negative then covalency is present, with the degree indicated by the magnitude of this quantity.[35,36] The $H(R)$ parameters for the M^+-RG_2 and M^+-RG complexes have been found to be positive for all of these species, leading to the conclusion that no covalency is present.

It is arguable whether atom-localized electron rearrangement (such as hybridization) is “chemical” or not; if it is taken that it is, then the presence of sp and sd hybridization in the present systems indicates chemical changes induced by the interaction of M^+ with the two RG atoms. This is in contrast to other species studied by our group, such as the B^+-Xe complex, which undergoes hybridization and also shows evidence of covalent bonding[10]; and the Au^+-Xe complex[37] where distinct evidence for covalency has been presented. Lastly, we note that we concluded that the M^+-He_2 and M^+-Ne_2 complexes are best described as an RG_2 unit interacting with the metal cation.

The titular complexes, when taken together with the two sets of lighter complexes, Be^+-RG_2 and Mg^+-RG_2 are a very interesting family, exhibiting different hybridizations and subtly-balanced energetics for the two main geometries exhibited: bent and linear.

Acknowledgements.

The authors are thankful to the EPSRC for computer time under the auspices of the NSCCS. A. A. (Grant # EP/H004815) and A. M. G. are grateful to the EPSRC and The University of Nottingham for the provision of DTA studentships. W. H. B is grateful to the Department of Chemistry at the University of Utah for travel funding, allowing visits to the University of Nottingham.

Table 1: Spectroscopic Parameters for the titular M^+-RG_2 Species[a]

RG	R_{e2}/Å	R_{e1}/Å	R_{e2}/R_{e1}	θ/°	$R_{RG\text{-}RG}$/Å	$R_e(RG_2)$	$R_{RG\text{-}RG}/R_e(RG_2)$	D_{e2}/cm^{-1}	D_{e1}/cm^{-1}	D_{e2}/D_{e1}
Ca^+										
He	4.302[b]	4.329	0.99	41.9	3.078	3.088	1.00	45 (41)	37 (35)	1.22 (1.17)
	4.05[c]			57.8[c]				101[c]		
Ne	3.772	3.708	1.02	49.5	3.158	3.166	1.00	159 (143)	133 (115)	1.20 (1.24)
	3.18[c]			67.0[c]				322[c]		
Ar	3.291	3.255	1.01	68.7	3.714	3.760	0.99	802 (776)	817 (765)	0.98 (1.01)
	3.172[d]			69.7[d]	3.623[d]			879[d]		
	3.20[c]			75.7[c]				1292[c]		
Kr	3.313	3.256	1.02	73.4	3.960	4.006	0.99	1187 (1165)	1304 (1232)	0.91 (0.95)
Xe	3.449	3.386	1.02	77.2	4.304	4.315	1.00	1691 (1739)	1944 (1897)	0.87 (0.92)
Rn	3.492	3.430	1.02	79.2	4.452	4.402	1.01	2038 (2111)	2390 (2344)	0.85 (0.90)
Sr^+										
He	4.583	4.606	1.00	39.8	3.120	3.088	1.01	38 (36)	30 (31)	1.27 (1.16)
Ne	3.991	4.005	1.00	46.6	3.157	3.166	1.00	142 (125)	112 (99)	1.27 (1.26)
Ar	3.497	3.447	1.01	64.3	3.721	3.760	0.99	679 (677)	663 (639)	1.02 (1.06)
Kr	3.412	3.454	0.99	180.0		4.006		985 (1029)	1057 (1016)	0.93 (1.01)
Xe	3.560	3.588	0.99	180.0		4.315		1397 (1513)	1573 (1561)	0.89 (0.97)
Rn	3.599	3.624	0.99	180.0		4.402		1731 (1875)	1948 (1947)	0.89 (0.96)
Ba^+										
He	4.963[b]	4.972	1.00	36.5	3.108	3.088	1.01	31 (28)	23 (23)	1.35 (1.22)
Ne	4.321	4.333	0.98	42.9	3.160	3.166	1.00	121 (104)	90 (78)	1.34 (1.33)
Ar	3.336	3.452	0.97	180.0		3.760		1050 (958)	702 (635)	1.50 (1.51)
Kr	3.429	3.506	0.98	180.0		4.006		1427 (1366)	1095 (1014)	1.30 (1.35)
Xe	3.597	3.660	0.98	180.0		4.315		1877 (1879)	1583 (1531)	1.19 (1.23)
Rn	3.661	3.711	0.99	180.0		4.402		2163 (2194)	1935 (1895)	1.12 (1.16)
Ra^+										
He	4.928	4.716	1.04	36.7	3.103	3.088	1.00	33 (31)	24 (22)	1.38 (1.41)
Ne	4.294	4.310	0.97	43.2	3.161	3.166	1.00	125 (109)	95 (83)	1.32 (1.31)
Ar	3.859	3.831	1.01	58.1	3.748	3.760	1.00	555 (566)	502 (496)	1.11 (1.14)
Kr	3.863	3.816	1.01	62.2	3.991	4.006	1.00	821 (838)	794 (773)	1.03 (1.08)
Xe	3.982	3.930	1.01	65.6	4.314	4.315	1.00	1172 (1258)	1182 (1188)	0.99 (1.06)
Rn	3.912	3.948	1.00	180.0		4.402		1480 (1552)	1480 (1497)	1.00 (1.04)

[a] R_{e2} is the M^+-RG equilibrium bond length in M^+-RG_2, R_{e1} is the M^+-RG equilibrium bond length in M^+-RG, and θ is the RG–M^+–RG bond angle. $R_{RG\text{-}RG}$ is the RG-RG internuclear distance in the M^+–RG_2 complex, and R_e (RG_2) is the optimized RG_2 R_e value. D_{e2} is the dissociation energy of M^+-RG …RG and D_{e1} is the dissociation energy of M^+…RG. The geometric parameter values were obtained at the RMP2/aug-cc-pVTZ level of theory. For the dissociation energies, the non-parenthesized values were obtained from RCCSD(T)/aug-cc-pVQZ calculations at the RMP2 optimized geometries, while the values in parentheses are those obtained from the RMP2 calculations (see text).

[b] For these two species, the optimized geometry had asymmetric structures, but the energy difference between them was very small (0.4 cm^{-1} for Ca^+-He_2 and 0.01 cm^{-1} for Ba^+-He_2), the optimized bond lengths were 4.329 Å and 4.276 Å for Ca^+-He_2 and 4.961 Å and 4.964 Å for Ba^+-He_2. The value in the table is the average of the two values in each case.

[c] B3LYP/6-311+G(3df), ref. 18.

[d] MP2 method with a (15s11p5d3f1g)/[12s9p5d3f1g] basis set for Ca and the standard aug-cc-pVQZ basis set for Ar. Ref. 17.

Table 2: Energy differences (cm^{-1}) between the linear and bent minima for M^+-RG_2 (M^+= Group 2; RG= He- Rn)[a]

	Metal Cation					
Rare Gas	**Be^+**	**Mg^+**	**Ca^+**	**Sr^+**	**Ba^+**	**Ra^+**
He	-9.6	-5.0	-16.3	-11.7	-6.4	-6.5
Ne	-86.4	-30.1	-60.4	-22.6	-22.1	-23.1
Ar	-1856.8	-349.3	-95.2	-20.8	321.9	-31.9
Kr	-2591.4	-521.3	-97.9	20.0	356.7	-10.7
Xe	-3120.3	-731.2	-160.0	9.8	455.9	-10.9
Rn	-2714.1	-705.3	-139.8	57.9	450.9	12.8

[a] A negative value indicates that the bent structure is the more stable.

[b] For Mg and Be with Rn angular plots were not calculated.

Table 3: Harmonic vibrational frequencies for M^+-RG_2 (M^+= Ca, Sr, Ba and Ra; RG_2 = He to Rn) species obtained at the RMP2/aug-cc-pVTZ level of theory (see text).[a]

Rare Gas	ν_1	ν_2	ν_3 /cm^{-1}
Ca^+			
He	74.6	49.7	76.7
Previous Work	62.3[a]	33.1[b]	54.3[b]
Ne	48.7	37.1	39.0
Previous Work	30.6[a]	22.2[b]	4.52[b]
Ar	62.7	36.4	46.1
Previous Work	71.1[a]	27.1[b]	42.7[b]
Kr	64.9	11.8	43.2
Xe	79.8	19.3	60.9
Rn	84.0	17.4	65.9
Sr^+			
He	24.0	17.0	20.8
Ne	26.7	15.3	11.9
Ar	50.4	37.6	39.5
Kr	39.1	28.2[c]	71.2
Xe	38.8	25.6[c]	71.1
Rn	31.8	22.0[c]	77.3
Ba^+			
He	28.2	17.6	33.9
Ne	19.8	42.2	12.7
Ar	65.2	23.7[c]	81.4
Kr	30.8	8.6[c]	68.3
Xe	51.0	39.3[c]	75.8
Rn	47.8	42.1[c]	80.1
Ra^+			
He	26.0	15.5	22.0
Ne	45.2	23.8	34.7
Ar	30.9	13.2	19.3
Kr	35.7	24.4	27.8
Xe	38.6	25.0	30.8
Rn	27.8	14.3[c]	46.7

[a] ν_1 and ν_2 correspond to the symmetric stretching and bending motions, but these motions are mixed for these two vibrations; ν_3 is the asymmetric stretch.

[b] B3LYP/6-311+G(3df), ref. 18.

[c] These values are doubly degenerate for the linear M^+-RG_2 complexes.

Table 4: Atomic Properties[a]

Species	Lowest Transition	Wavenumber of Lowest Transition[a]	Static Polarizability/ Å^3	Ionization Energy/ cm^{-1}
Ca^+	$^2D_{\frac{3}{2}}$ ($3p^6 3d$) ←$^2S_{\frac{1}{2}}$ ($3p^6 4s$)	13650	11[b]	
Sr^+	$^2D_{\frac{3}{2}}$ ($4p^6 4d$) ←$^2S_{\frac{1}{2}}$ ($4p^6 5s$)	14556	12.5[c]	
Ba^+	$^2D_{\frac{3}{2}}$ ($5p^6 5d$) ←$^2S_{\frac{1}{2}}$ ($5p^6 6s$)	4874	18.4[c]	
Ra^+	$^2D_{\frac{3}{2}}$ ($6p^6 6d$) ←$^2S_{\frac{1}{2}}$ ($6p^6 7s$)	12084	15.5[c]	
He			0.205	198311
Ne			0.396	173930
Ar			1.642	127110
Kr			2.519	112914
Xe			4.044	97834
Rn			5.103	86693

[a] Ref. 34

[b] Static dipole polarizabilities taken from ref. 1.

[c] Static dipole polarizabilities taken from ref. 33, where the CCSD(T) values are employed, since these give the best agreement with the value of 18 Å^3 for Ba^+ from ref. 1.

Table 5: Calculated charges on the metal centre, q_M, in M^+-RG_2 and M^+-RG[a]

	M^+-RG_2					M^+-RG			
	Ca^+	Sr^+	Ba^+	Ra^+		Ca^+	Sr^+	Ba^+	Ra^+
He	**1.01** [1.00] (1.00)	**1.00** [1.00] (1.00)	**1.00** [1.00] (1.00)	**1.00** [1.00] (1.00)		**1.00** [1.00] (1.00)	**1.00** [1.00] (1.00)	**1.00** [1.00] (1.00)	**1.00** [1.00] (1.00)
Ne	**1.02** [1.00] (0.98)	**1.02** [1.00] (0.99)	**1.02** [1.00] (0.99)	**1.02** [1.00] (0.99)		**1.01** [1.00] (0.99)	**1.01** [1.00] (0.99)	**1.01** [1.00] (0.99)	**1.01** [1.00] (0.99)
Ar	**1.04** [0.98] (0.94)	**1.04** [0.99] (0.95)	**1.02** [0.98] (0.97)	**1.04** [0.99] (0.95)		**1.02** [0.99] (0.97)	**1.02** [0.99] (0.97)	**1.02** [0.99] (0.97)	**1.02** [1.00] (0.97)
Kr	**1.03** [0.97] (0.94)	**1.04** [0.96] (0.98)	**1.01** [0.96] (1.00)	**1.03** [0.98] (0.94)		**1.02** [0.98] (0.96)	**1.02** [0.99] (0.97)	**1.01** [0.99] (0.96)	**1.02** [0.99] (0.97)
Xe	**1.01** [0.94] (0.89)	**1.02** [0.94] (0.91)	**0.98** [0.94] (0.95)	**1.02** [0.97] (0.91)		**1.00** [0.97] (0.93)	**1.01** [0.98] (0.93)	**1.00** [0.98] (0.94)	**1.01** [0.98] (0.95)
Rn	**1.00** [0.92] (0.82)	**1.02** [0.92] (0.81)	**0.98** [0.92] (0.88)	**1.01** [0.94] (0.87)		**1.00** [0.96] (0.89)	**1.00** [0.97] (0.88)	**0.99** [0.97] (0.90)	**1.00** [0.98] (0.91)

[a] AIM results presented in bold, NPA results are in square brackets, and Mulliken results are in parentheses. The charge on the RG atom can be found from $(1-q_M)/2$.

Table 6: Natural bond order analysis for the metal contributions to the HOMO for the M^+-RG_2 complexes[a]

	M^+					
RG	**Be**	**Mg**	**Ca**	**Sr**	**Ba**	**Ra**
Bent						
He	s (100%)	s (100%)	s (100.0%)	s (100.0%)	s (100.0%)	s (100.0%)
Ne	s (99.7%) p (0.29%)	s (99.96%) p (0.04%)	s (99.97%) p (0.02%) d (0.01%)	s (99.98%) p (0.01%) d (0.01%)	s (99.96%) p (0.01%) d (0.03%)	s (99.98%) p (0.01%) d (0.01%)
Ar	s (92.21%) p (7.77%) d (0.01%)	s (99.25%) p (0.75%)	s (99.17%) p (0.47%) d (0.36%)	s (99.36%) p (0.25%) d (0.36%)	s (96.15%) p (0.16%) d (3.69%)	s (99.58%) p (0.08%) d (0.34%)
Kr	s (92.22%) p (7.75%) d (0.01%)	s (98.96%) p (1.04%)	s (98.85%) p (0.66%) d (0.49%)	s (99.06%) p (0.36%) d (0.57%)	s (94.97%) p (0.22%) d (4.81%)	s (99.35%) p (0.10%) d (0.54%)
Xe	s (97.09%) p (7.86%) d (0.03%)	s (98.73%) p (1.26%) d (0.00%)	s (98.67%) p (0.81%) d (0.51%)	s (98.99%) p (0.40%) d (0.60%)	s (93.49%) p (0.20%) d (6.30%)	s (99.17%) p (0.12%) d (0.70%)
Rn	s (92.60%) p (7.34%) d (0.04%)	s (98.70%) p (1.29%) d (0.00%)	s (98.72%) p (0.78%) d (0.49%)	s (99.06%) p (0.35%) d (0.58%)	s (94.82%) p (0.16%) d (5.01%)	s (99.20%) p (0.0%) d (0.71%)
Linear						
He	[b]	[b]	s (100.0%)	s (100.0%)	s (100.0%)	s (100.0%)
Ne	[b]	[b]	s (99.98%) p (0.00% d (0.02%)	s (99.98%) p (0.00% d (0.02%)	s (99.94%) p (0.00% d (0.06%)	s (99.98%) p (0.00%) d (0.02%)
Ar	[b]	[b]	s (98.60%) p (0.00% d (1.40%)	s (98.42%) p (0.00% d (1.58%)	s (90.36%) p (0.00%) d (9.64%)	s (98.93%) p (0.00%) d (1.07%)
Kr	[b]	[b]	s (97.82%) p (0.00% d (2.18%)	s (97.72%) p (0.00%) d (2.28%)	s (90.01%) p (0.00%) d (9.99%)	s (98.28%) p (0.00%) d (1.72%)
Xe	[b]	[b]	s (97.55%) p (0.00% d (2.45%)	s (97.43%) p(0.00%) d (2.57%)	s (89.41%) p (0.0%) d (10.59%)	s (97.82%) p (0.00%) d (2.18%)
Rn	[b]	[b]	s (97.65%) p (0.00% d (2.35%)	s (97.54%) p (0.00%) d (2.46%)	s (90.33%) p (0.00%) d (9.67%)	s (97.84%) p (0.02%) d (2.16%)

[a] Small deviations from a total of 100% are associated with higher angular momentum functions and/or rounding errors.

[b] No symmetric RG-M^+RG minimum found.

Figure Captions:

Figure 1: Trends in R_{e2} and R_{e1} for the M^+- RG_n complexes (M^+= Ca, Sr, Ba and Rn and n = 1 or 2).

Figure 2: Selected minimum energy angular paths for selected Ca^+-RG_2, Sr^+-RG_2, Ba^+-RG_2 and Ra^+-RG_2 angular plots where a) RG =He b) RG= Ar and c) RG= Xe. (The zero on the interaction energy axis is for the M^+-RG + RG asymptote.) Each bond length was optimized independently, however for most angles this resulted in C_{2v} geometries; the exceptions were angles close to 0°

Figure 3: Trends in the D_{e2} and D_{e1} dissociation energies for the M^+- RG_n complexes (M^+= Ca, Sr, Ba and Rn and n = 1 or 2) .

Figure 4: Selected HF HOMO contour orbital diagrams for M^+-RG_2 (M^+= Ca, Sr, Ba and Ra; RG= He, Ar and Xe); the same contour values were used for all plots for ease of comparison. To indicate which contours correspond to the global minimum, we have identified these by underlining the chemical formula.

Figure 5: Minimum energy angular path for Ba^+-Xe_2 showing the change in the form of the HOMO contour.

Figure 1:

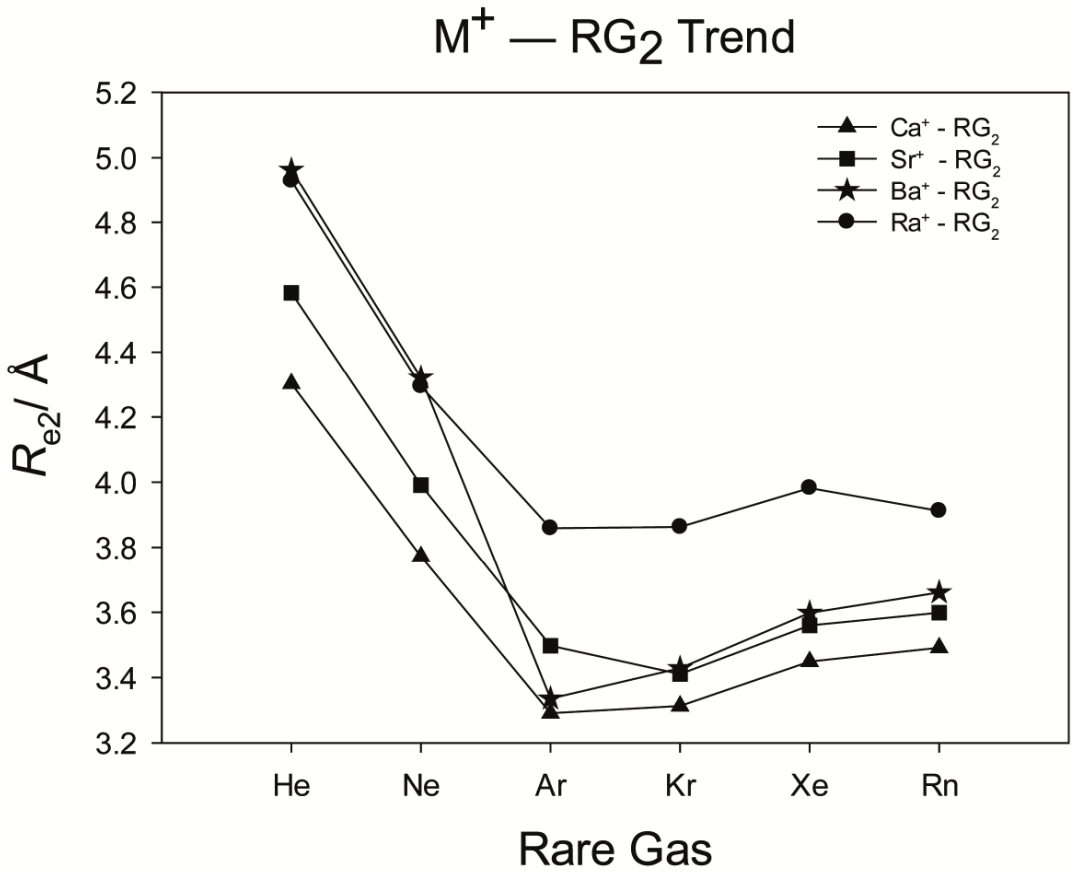
M+ — RG2 Trend
Ca+ - RG2
Sr+ - RG2
Ba+ - RG2
Ra+ - RG2
Re2/ Å
5.2
5.0
4.8
4.6
4.4
4.2
4.0
3.8
3.6
3.4
3.2
He
Ne
Ar
Kr
Xe
Rn
Rare Gas

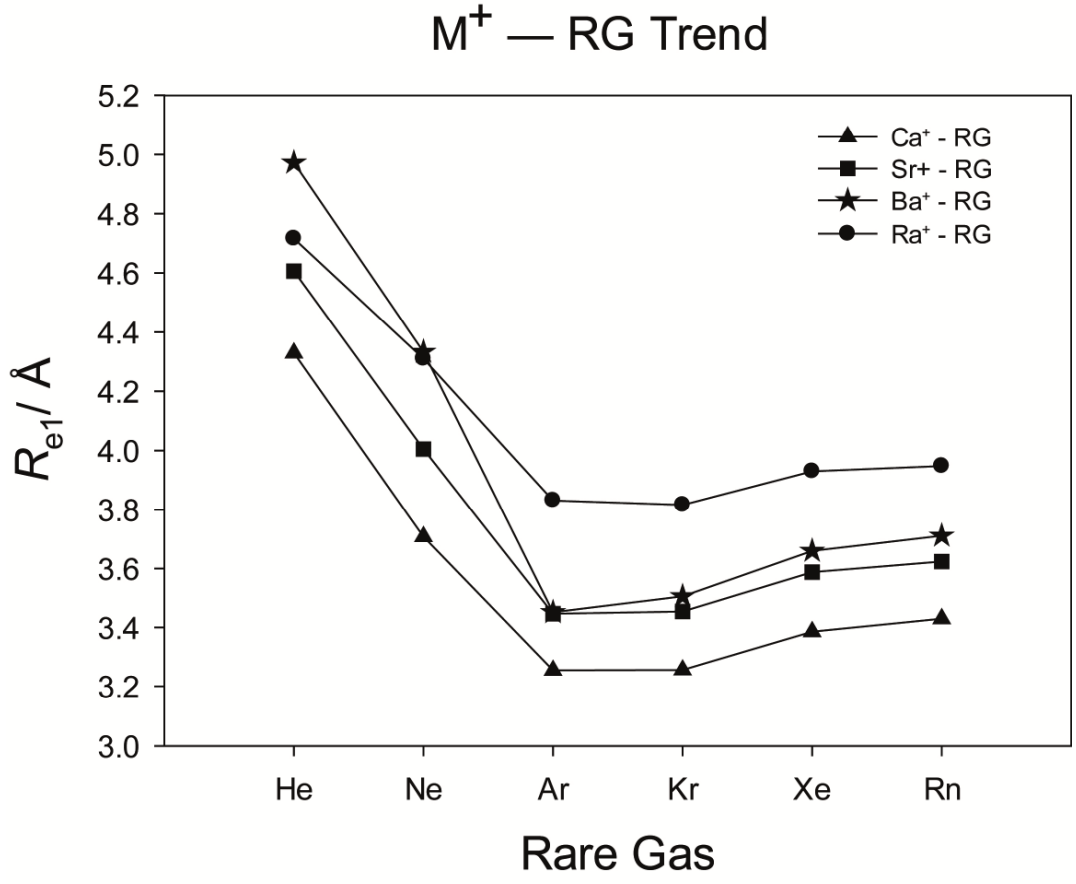
M+ — RG Trend
Ca+ - RG
Sr+ - RG
Ba+ - RG
Ra+ - RG
Re1/ Å
5.2
5.0
4.8
4.6
4.4
4.2
4.0
3.8
3.6
3.4
3.2
3.0
He
Ne
Ar
Kr
Xe
Rn
Rare Gas

Figure 2:

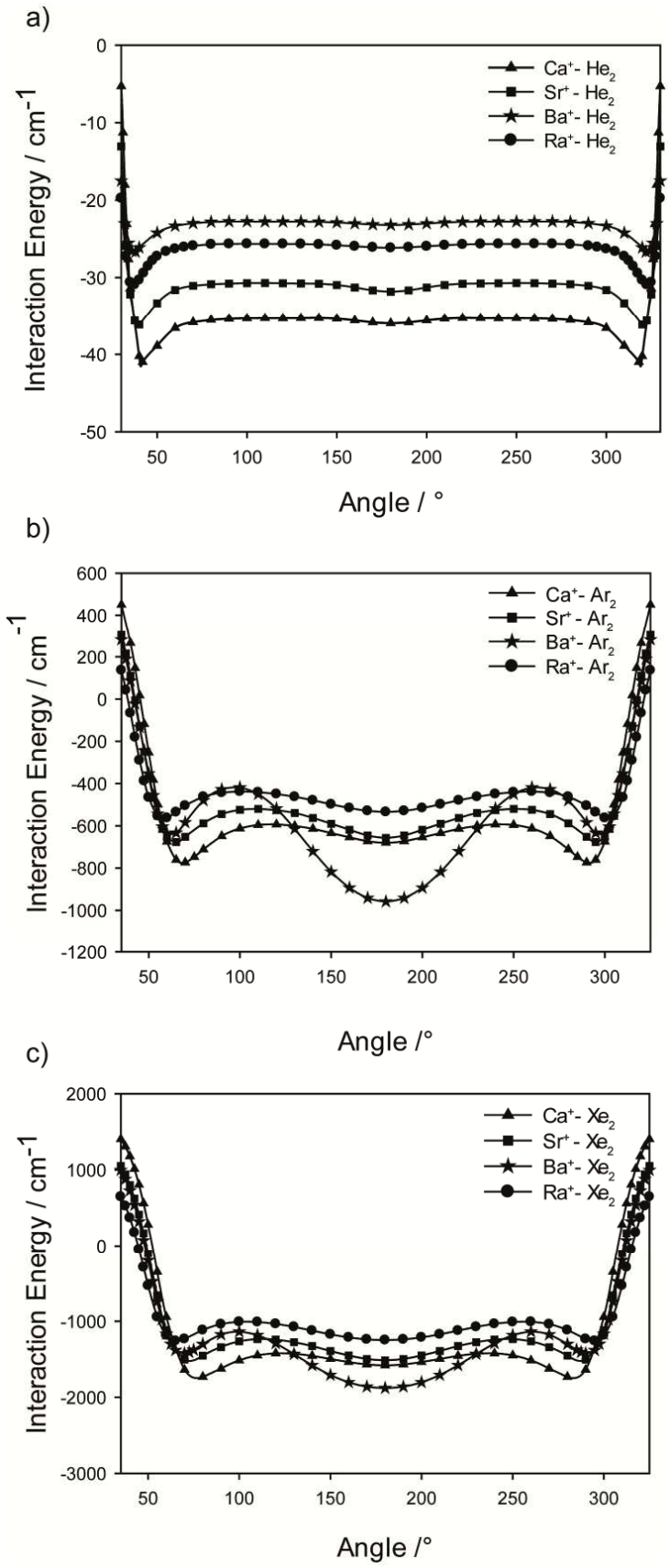
a)
Interaction Energy / cm-1
Angle / °
Ca+- He2
Sr+ - He2
Ba+- He2
Ra+- He2
b)
Interaction Energy / cm-1
Angle /°
Ca+- Ar2
Sr+ - Ar2
Ba+- Ar2
Ra+- Ar2
c)
Interaction Energy / cm-1
Angle /°
Ca+- Xe2
Sr+ - Xe2
Ba+- Xe2
Ra+- Xe2

Figure 3:

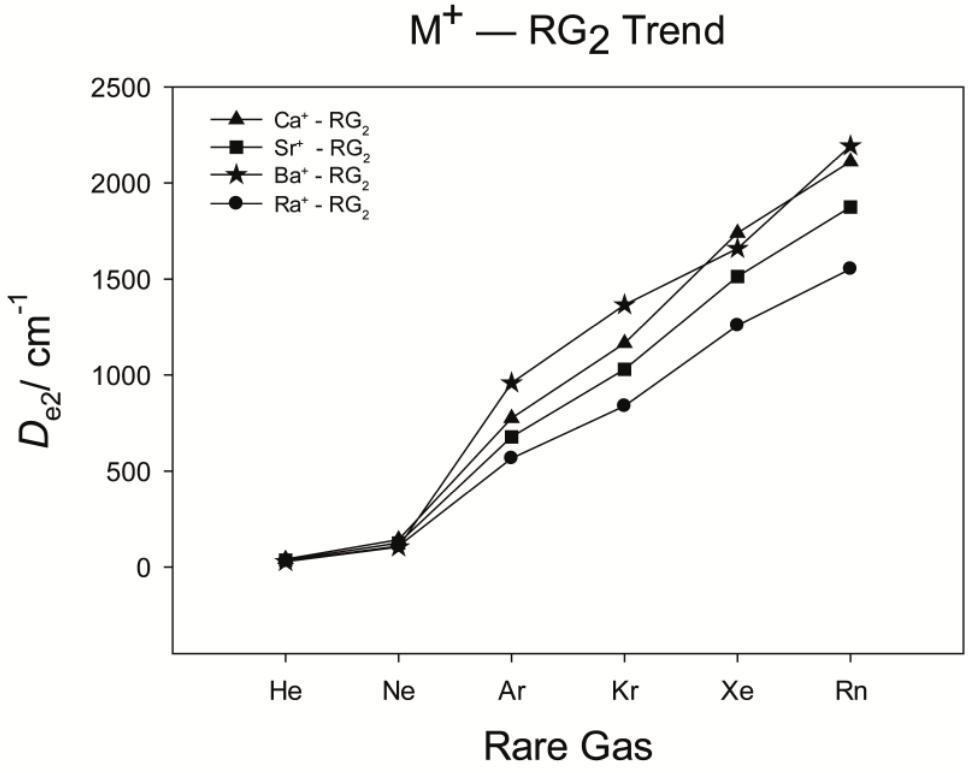
M+ — RG2 Trend
Ca+ - RG2
Sr+ - RG2
Ba+ - RG2
Ra+ - RG2
De2/ cm-1
2500
2000
1500
1000
500
0
He
Ne
Ar
Kr
Xe
Rn
Rare Gas

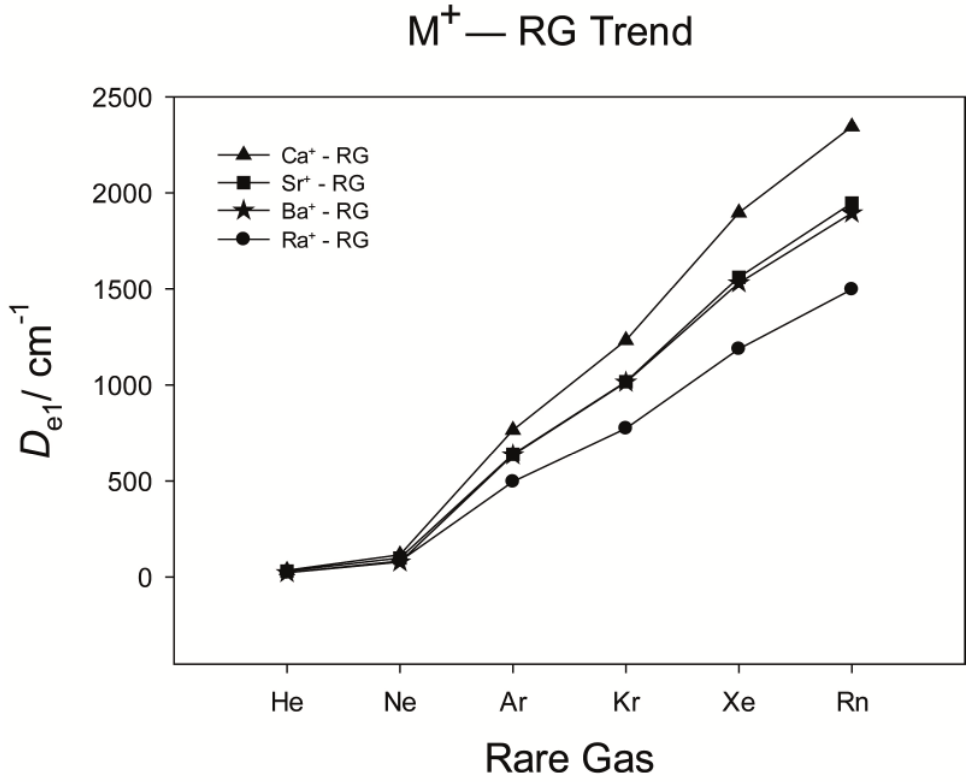
M+ — RG Trend
Ca+ - RG
Sr+ - RG
Ba+ - RG
Ra+ - RG
De1/ cm-1
2500
2000
1500
1000
500
0
He
Ne
Ar
Kr
Xe
Rn
Rare Gas

Figure 4:

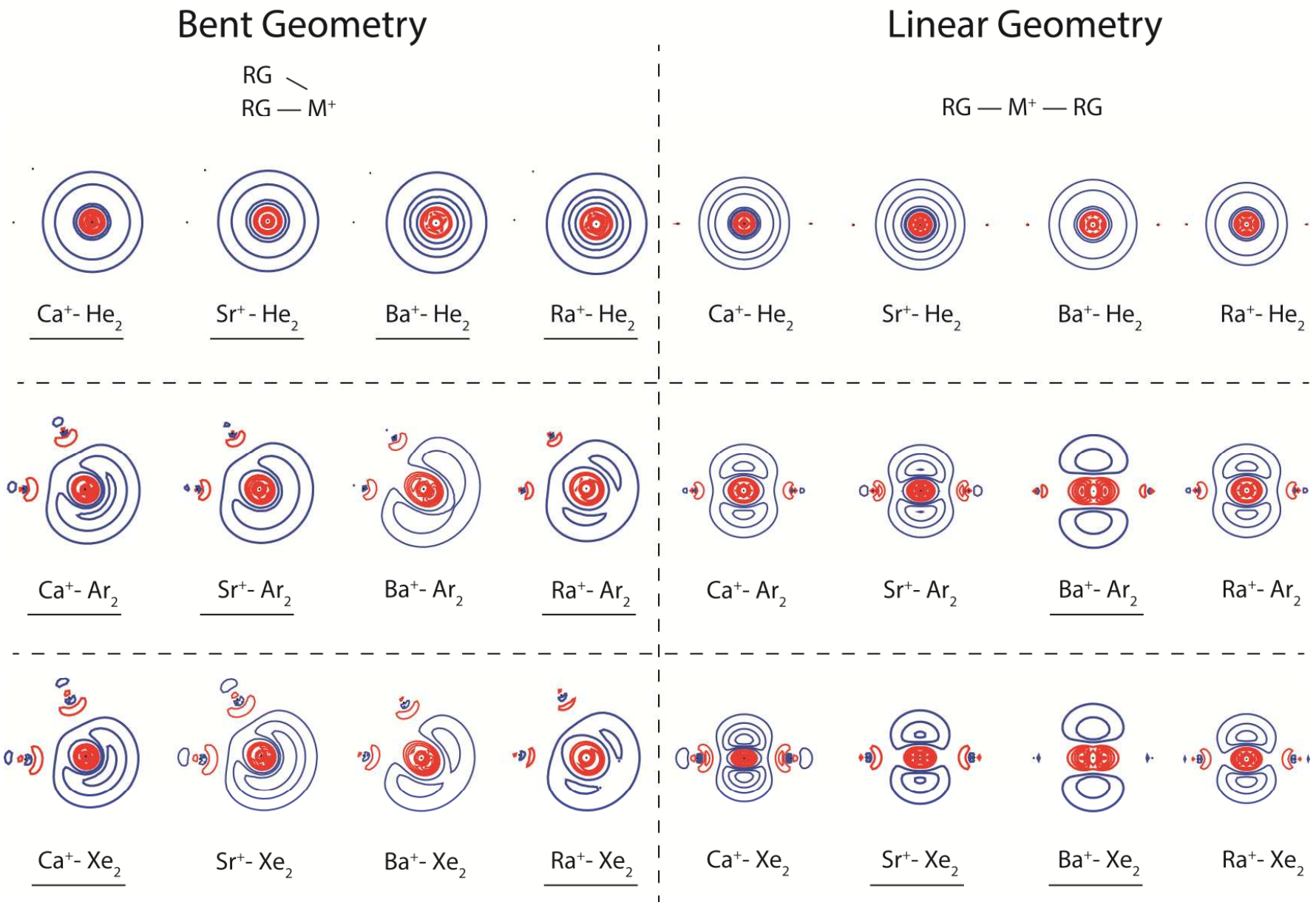
Bent Geometry
RG
RG — M+
Linear Geometry
RG — M+ — RG
Ca+- He2
Sr+ - He2
Ba+- He2
Ra+- He2
Ca+- He2
Sr+- He2
Ba+- He2
Ra+- He2
Ca+- Ar2
Sr+- Ar2
Ba+- Ar2
Ra+- Ar2
Ca+- Ar2
Sr+- Ar2
Ba+- Ar2
Ra+- Ar2
Ca+- Xe2
Sr+- Xe2
Ba+- Xe2
Ra+- Xe2
Ca+- Xe2
Sr+- Xe2
Ba+- Xe2
Ra+- Xe2

Figure 5:

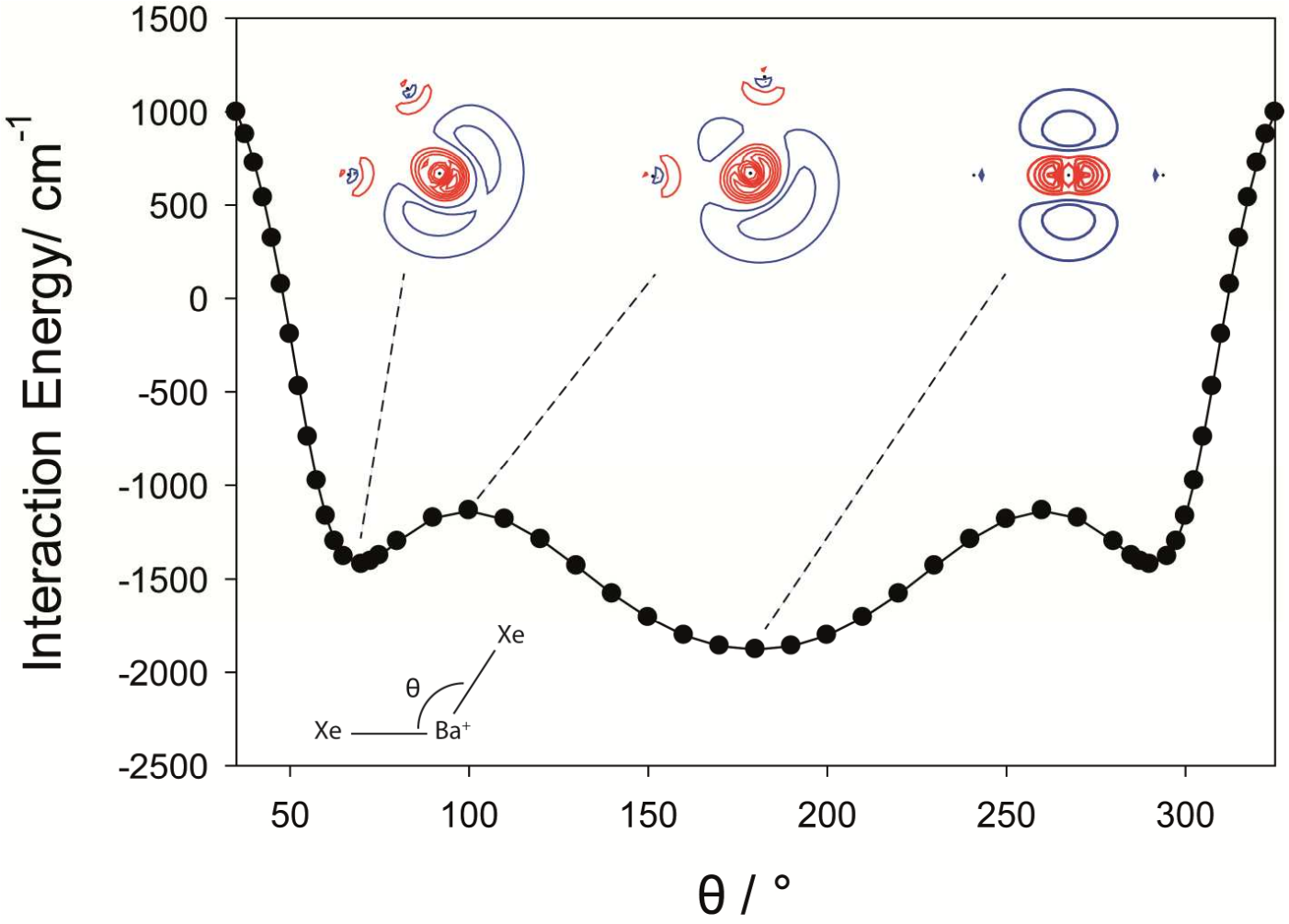
Interaction Energy/ cm-1
1500
1000
500
0
-500
-1000
-1500
-2000
-2500
50
100
150
200
250
300
θ / °
Xe
θ
Xe
Ba+

TOC GRAPHIC

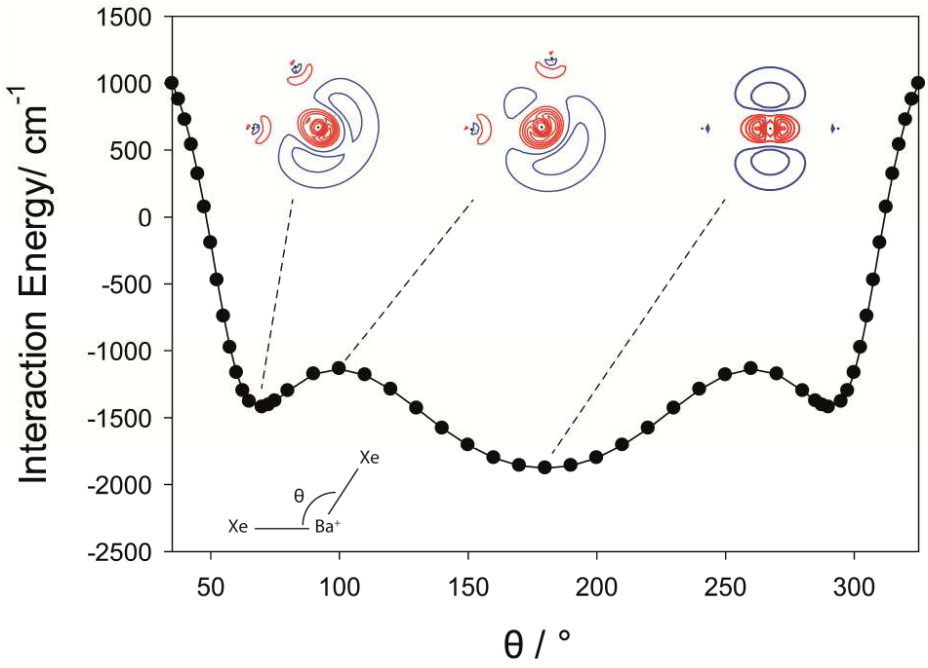
Interaction Energy/ cm-1
1500
1000
500
0
-500
-1000
-1500
-2000
-2500
50
100
150
200
250
300
θ / °
Xe
θ
Xe
Ba+

References

[1] Bellert, D.; Breckenridge, W. H. Bonding in Ground-State and Excited-State $A^{+}\cdot$ Rg van der Waals Ions (A= Atom, Rg = Rare-Gas Atom): A Model-Potential Analysis. *Chem. Rev*. **2002**, *102*, 1595-1622.

[2] Soldan, P.; Lee, E. P. F.; Lozeille, J.; Murrell, J. N.; Wright, T. G. High-Quality Interatomic Potential for $Li^{+}\cdot$He. *Chem. Phys. Lett*. **2001**, *343*, 429−436.

[3] Lozeille, J.; Winata, E.; Viehland, L. A.; Soldan, P.; Lee, E. P. F.; Wright, T. G. Spectroscopy of $Li^{+}\cdot$Rg and Li^{+}−Rg Transport Coefficients (Rg = He−Rn). *Phys. Chem. Chem. Phys*. **2002**, *4*, 3601−3610.

[4] Viehland, L. A.; Lozeille, J.; Soldan, P.; Lee, E. P. F.; Wright, T. G. Spectroscopy of $K^{+}\cdot$Rg and Transport Coefficients of K^{+} in Rg (Rg = He−Rn). *J. Chem. Phys*. **2004**, *121*, 341−351.

[5] Viehland, L. A.; Lozeille, J.; Soldan, P.; Lee, E. P. F.; Wright, T. G . Spectroscopy of $Na^{+}\cdot$Rg and Transport Coefficients of Na^{+} in Rg (Rg = He−Rn). *J. Chem. Phys*. **2003**, *119*, 3729−3736.

[6] Hickling, H. L.; Viehland, L. A.; Shepherd, D. T.; Soldan, P.; Lee, E. P. F.; Wright, T. G. Spectroscopy of $M^{+}\cdot$Rg and Transport Coefficients of M^{+} in Rg (M = Rb−Fr; Rg = He−Rn). *Phys. Chem. Chem. Phys*. **2004**, *6*, 4233−4239.

[7] Gardner, A. M.; Withers, C. D.; Wright, T. G.; Kaplan, K. I.; Chapman, C. Y. N.; Viehland, L. A.; Lee, E. P. F.; Breckenridge, W. H. Theoretical Study of the Bonding in M^{n+}-RG Complexes and the Transport of M^{n+} Through Rare Gas (M = Ca, Sr, and Ra; n = 1 and 2; and RG = He−Rn). *J. Chem. Phys*. **2010**, *132*, 054302−11.

[8] Gardner, A. M.; Withers, C. D.; Graneek, J. B.; Wright, T. G.; Viehland, L. A.; Breckenridge, W. H. Theoretical Study of M^{+}−RG and M^{2+}−RG Complexes and Transport of M^{+} through RG (M = Be and Mg, RG = He−Rn). *J. Phys. Chem. A* **2010**, *114*, 7631−7641.

[9] McGuirk, M. F.; Viehland, L. A.; Lee, E. P. F.; Breckenridge, W. H.; Withers, C. D.; Gardner, A. M.; Plowright, R. J.; Wright, T. G. Theoretical Study of Ba_n^{+}−RG (RG = Rare Gas) Complexes and Transport of Ba_n^{+} Through RG (n = 1,2; RG = He−Rn). *J. Chem. Phys*. **2009**, *130*, 194305−9.

[10] Harris J. P.; Gardner A. M.; Wright T. G. Interactions in the B^{+}-RG Complexes and Comparison with Be^{+}-RG (RG= He- Rn): Evidence for Chemical Bonding. *J. Phys. Chem. A* **2012**, *116*, 4995- 5007.

[11] Gray, B. R.; Lee, E. P. F.; Yousef, A.; Srestha, S.; Viehland; L. A.; Wright, T. G. Accurate Potential Energy Curves for Tl^{+}-Rg (Rg = He-Rn): Spectroscopy and Transport Coefficients, *Mol. Phys.* **2006**, *104*, 3237-3244.

[12] Gardner, A. M.; Gutsmiedl, K.; Wright, T. G.; Breckenridge, W. H.; Chapman, C. Y. N.; Viehland, L. A. Theoretical Study of Al^{+}-RG (RG = He-Rn), *J. Chem. Phys.* **2010**, *133* 164302-6.

[13] Gardner, A. M.; Gutsmiedl, K. A.; Wright, T. G.; Lee, E. P. F. ; Breckenridge, W. H.; Rajbhandari, S.; Chivone, C. Y. N.; Viehland, L. A. Theoretical Study of M^{+}-RG Complexes (M = Ga, In; RG = He-Rn), *J. Phys. Chem. A* **2011**, *115* 6979-6985.

[14] Bauschlicher, C. W., Jr.; Partridge, H.; Langhoff, S. R. Comparison of the Bonding Between ML^{+} and ML_2^{+} (M = Metal, L= Noble Gas). *Chem. Phys. Lett*. **1990**, *165*, 272−276.

[15] Andrejeva, A.; Gardner, A. M.; Graneek, J. B.; Plowright, J. R.; Breckenridge, W. H.; Wright, T. G. Theoretical Study of M^{+}−RG_2 (M^{+} = Li, Na, Be, Mg; RG = He−Rn). *J. Phys. Chem. A* **2013**, *117*, 13578 – 13590.

[16] Duncan, M. A. Spectroscopy of Metal Ion Complexes: Gas-Phase Models for Solvation. *Annu. Rev. Phys. Chem.* **1997**, *48*, 69-93.

[17] Velasquez, J.; Kirschner, K. N.; Reddic, J. E.; Duncan, M. A. Ca^{+}-Ar_2 Complexes: Linear or Bent? *Chem. Phys Lett*. **2001**, *343*, 613- 621.

[18] Jalbout, A. F.; Solimannejad, M. Density Functional Theory Analysis of $CaRg_n^{+}$ Complexes: (Rg = He, Ne, Ar; *n* = 1–4). *J. Molec. Struct. (Theochem)* **2003**, *640*, 21–23.

[19] Fanourgakis, G. S.; Farantos, S. C.; Lüder, Ch.; Velegrakis, M.; Xantheas, S. S Photofragmentation Spectra and Structures of $Sr^{+}Ar_n$, n=2 – 8 Clusters: Experiment and Theory *J. Chem. Phys*. **1998**, *109*, 108- 120.

[20] Fanourgakis, G. S.; Farantos, S. C.; Lüder, C.; Velegrakis, M.; Xantheas, S. S. Photofragmentation Spectra and Potential Energy Surfaces of $Sr^{+}Ar_2$. *Phys. Chem. Chem. Phys*. **1999**, *1*, 977 -981.

[21] MOLPRO, version 2012.1, a package of ab initio programs, Werner, H.-J.; Knowles, P. J.; Knizia, G.; Manby, F. R.; Schütz, M.; et al. see http://www.molpro.net.

[22] Peterson K.A.; Figgen,D.; Goll, E.; Stoll,H.; Dolg, M. Systematically Convergent Basis Sets with Relativistic Pseudopotentials. II. Small-Core Pseudopotentials and Correlation Consistent Basis Sets for the Post-*d* Group 16–18 elements *J. Chem. Phys.* **2003** *119*, 11113-11123.

[23] DeYonker, N. J.; Peterson, K. A.; Wilson, A. K. Systematically Convergent Correlation Consistent Basis Sets for Molecular Core−Valence Correlation Effects: The Third-Row Atoms Gallium through Krypton *J. Phys. Chem A* **2007**, *111*, 11383-11393.

[24] Private communication, Prof. Kirk A. Peterson, Washington State University, also briefly described in: Li, H.; Feng, H.; Sun, W.; Zhang, Y.; Fan, Q.; Peterson, K.A.; Xie, Y.; Schaefer, H.F. III, The Alkaline Earth Dimer Cations (Be_2^{+}, Mg_2^{+}, Ca_2^{+}, Sr_2^{+}, and Ba_2^{+}). Coupled Cluster and Full Configuration Interaction Studies *Molec. Phys.* 2013, *111*, 2292 (2013).

[25] Lim, I. S.; Stoll, H.; Schwerdtfeger, P. Relativistic Small-Core Energy-Consistent Pseudopotentials for the Alkaline-Earth Elements from Ca to Ra *J. Chem. Phys.* **2006**, *124*, 034107-9.

[26] Gaussian 09, Revision D.01, Frisch, M. J.; Trucks, G. W.; Schlegel, H. B.; Scuseria, G. E.; Robb, M. A.; Cheeseman, J. R.; Scalmani, G.; Barone, V.; Mennucci, B.; Petersson, G. A.et al.Gaussian, Inc., Wallingford CT, 2009.

[27] Glendening, E. D.; Badenhoop, J. K.; Reed, A. E.; Carpenter, J. E.; Bohmann, J. A.; Morales, C. A.; Landis, C. R.; Weinhold, F. NBO 6.0, Theoretical Chemistry Institute, University of Wisconsin, Madison, **2013**.

[28] Kirschner, K. N.; Ma, B.; Bowen, J. P.; Duncan, M. A. Theoretical Investigation of the Ca^{+}-N_2 and Ca^{2+} -N_2 Complexes. *Chem. Phys. Lett*. **1998**, *295*, 204 - 210.

[29] Mulliken, R. S.; Electronic Population Analysis on LCAO-MO Molecular Wave Functions. I. *J. Chem. Phys*.**1955**, *23*, 1833-1840.

[30] Reed, A. E.; Weinstock, R. B.; Weinhold, F. Natural Population Analysis. *J. Chem. Phys*. **1985**, *83*, 735-746.

[31] Bader, R. F. W. *Atoms in Molecules- A Quantum Theory*, Oxford University Press: Oxford, U. K. **1990.**

[32] P. Soldán, E. P. F. Lee and T. G. Wright**,** Static Dipole Polarizabilities (α) and Static Second Hyperpolarizablities (γ) of the Rare Gas Atoms (He-Rn)", *Phys. Chem. Chem. Phys.* **2001**, *3*,4661-4666.

[33] Sahoo, B. K.; Timmermans, R. G. E.; Das, B. P.; Mukherjee, D. Comparative Studies of Dipole Polarizabilities in Sr^+, Ba^+, and Ra^+ and their Applications to Optical Clocks**,** *Phys. Rev. A***,** 2009**,** *80***,** 062506-10.

[34] Kramida, A.; Ralchenko, Yu.; Reader, J. and NIST ASD Team (2014). NIST Atomic Spectra Database (ver. 5.2), [Online]. Available: http://physics.nist.gov/asd [2014, November 14]. National Institute of Standards and Technology, Gaithersburg, MD.

[35] Cremer, D.; Kraka, E. Chemical Bonds without Bonding Electron Density- Does the Difference Electron-Density Analysis Suffice for a Description of the Chemical Bond? *Angew. Chem. Int. Ed. Engl*. **1984**, *23*, 627-628.

[36] Nakanishi, W.; Hayashi, S.; Narahara, K. Polar Coordinate Representation of $H_b(r_c)$ versus $\left(\frac{\hbar^2}{8m}\right)\nabla^2\rho_b(r_c)$ at BCP in AIM Analysis: Classification and Evaluation of Weak to Strong Interactions *J. Phys. Chem. A* **2009**, *113*, 10050-10057.

[37] Wright, T. G.; Breckenridge W. H.; Ayles V. L. Evidence for Emergent Chemical Bonding in Au^+-Rg Complexes (Rg = Ne, Ar, Kr, and Xe) *J. Phys. Chem. A* **2008**, *112*, 4209-4214.